Chandra view of the dynamically young cluster of galaxies A1367 II. point sources

M. Sun & S. S. Murray

Harvard-Smithsonian Center for Astrophysics, 60 Garden St., Cambridge, MA 02138; msun@cfa.harvard.edu

ABSTRACT

A 40 ks *Chandra* ACIS-S observation of the dynamically young cluster A1367 yields new insights on X-ray emission from cluster member galaxies. We detect 59 point-like sources in the ACIS field, of which 8 are identified with known cluster member galaxies. Thus, in total 10 member galaxies are detected in X-rays when three galaxies discussed in paper I (Sun & Murray 2002; NGC 3860 is discussed in both papers) are included. The superior spatial resolution and good spectroscopy capability of *Chandra* allow us to constrain the emission nature of these galaxies. Central nuclei, thermal halos and stellar components are revealed in their spectra. Two new low luminosity nuclei (LLAGN) are found, including an absorbed one (NGC 3861). Besides these two for sure, two new candidates of LLAGN are also found. This discovery makes the LLAGN/AGN content in this part of A1367 very high ($\gtrsim$ 12%). Thermal halos with temperatures around 0.5 - 0.8 keV are revealed in the spectra of NGC 3842 and NGC 3837, which suggests that Galactic coronae can survive in clusters and heat conduction must be suppressed. The X-ray spectrum of NGC 3862 (3C 264) resembles a BL Lac object with a photon index of ~ 2.5. We also present an analysis of other point sources in the field and discuss the apparent source excess ($\sim 2.5\ \sigma$) in the central field.

Subject headings: galaxies: clusters: general — galaxies: clusters: individual (A1367) — galaxies: active — magnetic fields — X-rays: galaxies

1. Introduction

Galaxies can generally be divided into field galaxies and those in groups or clusters. Both types are known as X-ray emitters from at least the *Einstein* era (Marshall et al. 1978). A comparison of the X-ray emission of galaxies in different type of clusters, and a comparison with field galaxies, can tell us the effect of environment on the evolution of galaxies and can further provide

some insights into the evolution of clusters. To achieve that, we need to study the X-ray emission of galaxies in different types of clusters. However, limited by the X-ray instruments little work has been done in this field for clusters more distant than the Virgo cluster (e.g., Dow & White 1995; Sakelliou & Merrifield 1998). In this paper, we present the X-ray analysis of the point sources detected in a 40 ks *Chandra* observation of A1367, with special emphasis on the sources associated with member galaxies. Three extended sources associated with member galaxies are discussed in paper I.

A1367 is a nearby irregular cluster (z=0.022) with many substructures in X-rays (Bechtold et al. 1983, B83 hereafter; Grebenev et al. 1995, G95 hereafter; Lazzati et al. 1998, L98 hereafter; paper I). A complete flux limited sample of X-ray sources associated with the cluster is important in understanding the effects of environment on galaxy properties and evolution. Previous analyses based on *Einstein* HRI (EHRI hereafter) and *ROSAT* PSPC (B83; G95; L98) found 47 point sources in total, associated with member galaxies or not. However, the results from these analyses have been inconsistent, especially in the overlap of detected sources. The inconsistencies are most likely due to the relatively poor quality of the EHRI data, or the low angular resolution of the PSPC data.

Now with *Chandra*'s superior spatial resolution, wider energy coverage, better spectral resolution and sensitivity than EHRI and PSPC, we not only can detect more point sources in the field, but also study the spectra of bright ones. *Chandra* data reduction is described in §2. A summary of the point sources detected is in §3. In §4 the properties of detected cluster member galaxies are discussed. Other interesting point sources are described in §5. §6 discusses the source excess observed in the central field. Throughout this paper, we assume h=0.5 (H_0 = 100h km s^{-1} Mpc^{-1}) and q_0 = 0.5. These cosmological parameters correspond to the linear scale of 0.62 kpc/arcsec at the cluster redshift. All luminosities scale as $h_{0.5}^{-2}$.

2. *Chandra* observations & data reduction

A1367 was observed on February 26, 2000 by *Chandra* with the Advanced CCD Imaging Spectrometer (ACIS). The observation was taken by the ACIS-S instrument. This observation contains three particle background flares that were excluded based on the X-ray light curves from the outer parts of the field. After excluding the period of background flares, the effective exposures are 37.8 ks for the S1 and S3 chips, 37.4 ks for the S2 and S4 chips, and 39.0 ks for the I2 and I3 chips. The procedure of the data reduction has been mentioned in paper I. Here we will only state those specific of the purpose of this paper. CIAO WAVDETECT was used to detect point sources. Absolute positions of X-ray sources were carefully checked using optical identifications. A small boresight error of $\sim 2''$ in the original data was corrected. The derived positions are accurate to $\sim 0.5''$ near the aimpoint, with larger errors further out. In this work, all the background used is the

local background. CIAO(2.1), FTOOLS(5.0) and XSPEC(11.0) were used for the data reduction.

The calibration data used correspond to CALDB 2.9 from *Chandra* X-ray Center (CXC). The errors in this paper are 90% confidence interval. The properties of member galaxies are from the NASA Extragalactic Database (NED). A Galactic absorption of 2.2×10^{20} cm^{-2} was used in the spectral fitting unless otherwise specified.

3. Summary of the point sources

Fig. 1 shows the photon image of this observation. The field of view (FOV) of this observation is shown in Fig. 2 of paper I. We ran CIAO WAVDETECT on different scales to detect point sources. The probability of erroneously associating a background fluctuation in a pixel with a detection was set at 10^{-6}, which produces less than 1 false detections per 4 chips field (Freeman et al. 2002). To maximize signal to noise ratio, only data in the 0.5 - 7 keV band were used. MKPSF in CIAO was used to check the point-like nature of the detected sources. Since the sizes of PSFs depend on energy, for bright sources (> 50 counts) we fit their spectra and considered the effect of energy on the PSF sizes for them. In total, 59 point sources in the field were detected. Eight of them are known member galaxies (Table 1). All point sources are shown in Fig. 2 and their properties are presented in Table 2 (except the ones corresponding to the known member galaxies and QSOs, which are discussed in §4 and §5.1 respectively). The aperture photometry method (e.g., Giacconi et al. 2001) was applied to obtain the count rates of these point sources in the soft (0.5 - 2 keV) and hard (2 - 7 keV) band respectively. The radius of the aperture is chosen to be the 90% encircled energy average radius (EEAR) of the local PSF. The correction on the exposure map (including vignetting) has been applied. Thus, we can convert the count rates to fluxes just based on the response files at the aimpoint. Assuming a power law with a photon index of 1.7 (1.5 - 2.0) and a Galactic absorption, the minimum detectable fluxes are $\sim$ 1.4 (1.4) $\times10^{-15}$ ergs cm^{-2} s^{-1} in the 0.5 - 2 keV band and 0.8 (1.1 - 0.5) $\times$ 10^{-14} ergs cm^{-2} s^{-1} in the 2 - 10 keV band (we measured 2 - 7 keV count rates and converted them to 2 - 10 keV fluxes). At the distance of A1367 (z=0.022), these fluxes correspond to 2.9 (2.9) $\times10^{39}$ ergs s^{-1} (0.5 - 2 keV) and 1.7 (2.3 - 1.1) $\times$ 10^{40} ergs s^{-1} (2 - 10 keV). Although the ACIS field is full of the cluster emission, A1367 is a relatively low X-ray-surface-brightness cluster so that the effect on point source detection is small (at most raise the detection limits by $\sim$ 40% around cluster center).

Forty-five of these fifty-nine sources are new. There are 8 known member galaxies and 3 known QSOs. Of the 48 remaining sources, 21 have optical counterparts in DSS II, 2 have radio counterparts in Gavazzi & Contursi (1994; GC94 hereafter), and 25 sources have no counterparts in either DSS II or GC94.

We also checked the point sources detected by previous EHRI and PSPC observations (B83, G95 and L98). The sensitivity of this *Chandra* observation should allow us to detect all of them if they are real and not highly variable. The results are presented in Table 3. For 27 previously detected point sources in the ACIS FOV (of 47 in total), only 14 are confirmed. Almost all sources not confirmed by *Chandra* are EHRI sources. Moreover, all these EHRI sources without *Chandra* detection were also not detected by the *ROSAT* PSPC. This fact is very similar to what we found for extended sources claimed by previous observations (paper I). These EHRI point sources were generally detected at $\sim 3\ \sigma$ levels (G95). However, as we mentioned in paper I, the EHRI observations of A1367 may not be well calibrated so that some background fluctuations were regarded as sources.

4. Point Sources associated with known member galaxies

Eight of fifty-nine point sources are associated with member galaxies (Table 1). In total, 10 member galaxies are detected in this observation. NGC 3860 has a point component and an extended one, while UGC 6697 and NGC 3860B are both extended in X-rays (paper I). Five sources are located over $10'$ from the aimpoint, thus any structure on scales $\lesssim 10''$ is smeared out by the degraded PSFs at large off-axis angles. For the galaxies not detected, this observation puts $3\ \sigma$ upper limits of 0.3 - 4.7×10^{40} ergs s^{-1} (0.5 - 2 keV) for the point-like emission from them (Table 1). In the following, we discuss the eight point-like sources associated with known member galaxies respectively.

4.1. E and S0 galaxies

1) NGC 3862 (3C 264)

It is a bright radio source (3C 264) with a clear jet-like structure (Bridle & Vallée, 1981). Its optical spectrum is that of a normal elliptical galaxy with only one very weak emission line [N II] and no detectable Balmer emission (Elvis et al. 1981). Elvis et al. (1981) suggested that its nucleus was similar to a low-luminosity BL Lac object based on its strong nuclear X-ray emission revealed by *Einstein* and basically featureless optical spectrum. Crane et al. (1993) discovered a sub-arcsec optical synchrotron jet by *HST*.

In this observation, the galaxy is in the S4 chip and unresolved (the 50% EEAR of PSF there is $\sim 8''$). About 9000 counts were collected. The 0.7 - 9 keV spectrum is featureless and well

fit by a power law with photon index of 2.44±0.05 modified by the Galactic absorption (χ^2 = 126.4/124; Fig. 3). A thermal plasma model (e.g., MEKAL) fits it poorly. A broken power law or any additional thermal component besides the power law does not significantly improve the fit. The unabsorbed X-ray luminosity (0.5 - 10 keV) is 4.1×10^{42} ergs s^{-1}. The contribution from LMXB is at most 4% scaling from the LMXB X-ray-to-optical ratios in Sarazin, Irwin & Bregman (2001; S01 hereafter). The source appears constant in intensity. The 2 - 10 keV luminosity 1.5×10^{42} ergs s^{-1} is typical for Radio galaxies (Sambruna, Eracleous & Mushotzky 1999). The 2 - 10 keV spectra of AGNs (including Seyferts, QSOs and Radio galaxies) are rather homogeneously represented by a power law with photon index of 1.7 - 2.0 (e.g., Nandra & Pounds 1994; Sambruna et al. 1999). However, for NGC 3862, even if only 2 - 9 keV spectrum is fitted, the photon index is large at $2.72^{+0.19}_{-0.18}$ (χ^2 = 28.4/41). The spectrum of NGC 3862 is similar to the steep spectra found in BL Lac objects (photon index $\sim$ 2.5; e.g., Ciliegi, Bassani & Caroli 1995; Kubo et al. 1998).

2) NGC 3842

In optical this is the brightest galaxy in the field and also the cD galaxy of a galaxy concentration around it. In this observation, it is 13.9′ off-axis in the S1 chip. The position of the X-ray source agrees with the optical nucleus. About 900 net counts were collected in this observation. No significant variations in its lightcurve were detected. Its spectrum cannot be described well by one component, either a power law or a MEKAL. At least two components, a soft and a hard, are needed (Fig. 4). The soft component can be well described by a MEKAL model (the abundance is fixed to 0.5 solar), while a power law and a thermal Bremsstrahlung both can fit the hard component well (χ^2 are $\sim$ 15.7/19). If a Bremsstrahlung is adopted for the hard component, the best-fit temperature of the soft component is $0.70^{+0.08}_{-0.05}$ keV and the temperature of the hard component is $2.9^{+3.9}_{-1.3}$ keV. If a power law is adopted, the temperature of the soft component is 0.73±0.07 keV while the photon index of the hard component is $2.1^{+0.7}_{-0.4}$. In each case, the total luminosity in the 0.5 - 10 keV band is 1.9×10^{41}ergs s^{-1}, while the luminosity of the soft component is about same - 9×10^{40} ergs s^{-1} (0.5 - 10 keV). The luminosity ratio of the hard X-ray component to the optical L_{hard} (0.3 - 10 keV) / L_B is 6.8×10^{29} ergs s^{-1} $L^{-1}_{B\odot}$, which is quite similar to the values presented in S01 — 8.1, 7.2×10^{29} ergs s^{-1} $L^{-1}_{B\odot}$ for NGC 4697 (E) and NGC 1553 (S0) respectively. This suggests the hard component may be dominated by X-ray binaries. The soft component is naturally explained as the thermal halo of NGC 3842. The upper limit of the halo size is $\sim 12''$ in radius.

3) NGC 3837

In this observation, it is 12.4′ off-axis (the 50% EEAR of PSF is $\sim 13''$ there) in the S1 chip and unresolved. About 400 counts from it were collected. No significant variations in its *Chandra* lightcurve were found. Its X-ray spectrum clearly shows at least two components: a soft one and a hard one dominant above 2-3 keV (Fig. 4). A MEKAL model is used to represent the

soft component, which may be a thermal halo. The hard component has a rather flat spectrum. One possibility of the hard component is the combination of X-ray binaries. To follow S01, we used a 8 keV thermal Bremsstrahlung to represent the hard component. The abundance in the MEKAL model for the soft component is fixed to 0.5 solar. The fitting result is acceptable with χ^2 of 14.4/13. The temperature of the soft component is $0.60^{+0.07}_{-0.12}$ keV, which is not sensitive to the assumed model for the hard component. The derived L_x (0.5 - 10 keV) is 4.4×10^{40} ergs s^{-1} for the soft component and 4.8×10^{40} ergs s^{-1} for the hard one. The luminosity ratio of the hard component and the optical L_x (0.3 - 10 keV)/L_B is 1.2×10^{30} ergs s^{-1} $L^{-1}_{B\odot}$, consistent with the results in S01. If we change the assumed temperature of the hard component to 5 - 10 keV, the results do not change much.

4) CGCG 097-109

This is the first X-ray detection of this source, while the previously claimed detections Be5 (B83), Gp11* and Ge14 (G95) are actually the nearby bright point source 15 (Fig. 2). In this observation, it is a point-like source and the position agrees with the optical nucleus of the galaxy within $0.5''$. The superior spatial resolution of *Chandra* puts an upper limit $\sim 0.5h^{-1}_{0.5}$ kpc to the size of the X-ray emitting source. Though only ~ 50 counts were collected, a spectral fit is performed. A power law model with photon index $2.3^{+1.2}_{-0.7}$ modified by the Galactic absorption gives satisfied results while the thermal plasma models (e.g., MEKAL) fit the data poorly. The derived L_x is 1.5×10^{40} ergs s^{-1} (0.5 - 10 keV) and 6×10^{39} ergs s^{-1} (2 - 10 keV). The scaled X-ray luminosity of the LMXB component is 1.9-2.1$\times10^{40}$ ergs s^{-1} (0.3 - 10 keV) based on the results in S01, which is comparable to the value we found. However, the LMXB component should follow the optical light of the galaxy, which has a size of $\sim 20''$. The source found is point-like with an upper limit of only $\sim 1''$. Thus, this X-ray source is more likely the LLAGN of CGCG 097-109. The possibility of an ULX source is low since ULXs usually occur in regions of star formation (e.g., Fabbiano, Zezas & Murray 2001). The LMXB component is most likely swamped into the surrounding ICM emission. Assuming a typical spectrum (8 keV Bremsstrahlung) for the LMXB component in CGCG 097-109, the 3 σ upper limit on the luminosity of an extended source (in $20''$ radius - the optical size) surrounding the nucleus is 2.7×10^{40} ergs s^{-1} (0.3 - 10 keV), which is above the luminosity that is expected from LMXBs in this galaxy.

5) CGCG 097-113

This is the first X-ray detection of this source. Only ~ 18 counts are collected from this source and the upper limit on the size of the X-ray emitter is $\sim 2''$. The position agrees with the optical nucleus of the galaxy within $1''$. Its 0.5 - 10 keV luminosity is estimated to be 4 - 9 $\times10^{39}$ ergs s^{-1} assuming a photon index of 1.7 - 2.5. The scaled X-ray luminosity of the LMXB component is 1.1-1.2$\times10^{40}$ ergs s^{-1} (0.3 - 10 keV) based on the results in S01. However, the optical size of the

galaxy ($\sim 15''$) is much larger than the size of the X-ray emitter. Thus, the observed X-ray source is more likely a LLAGN, while the possibility of an ULX source is low as we mentioned above for CGCG 097-109. Assuming a typical spectrum (8 keV Bremsstrahlung) for the LMXB component in CGCG 097-113, the 3 σ upper limit on the luminosity of an extended source (in $15''$ radius - the optical size) surrounding the nucleus is 1.9×10^{40} ergs s^{-1} (0.3 - 10 keV), which is above the luminosity that is expected from LMXBs in this galaxy.

4.2. Spiral galaxies

6) NGC 3861

In optical NGC 3861 has a bright nucleus (Fig. 2). It was classified as one of the three "red galaxies" by Schommer & Bothun (1983) based on the optical colors. These kinds of galaxies were considered to have non-continuing star formation activity. In this observation, it is $\sim 14.1'$ off-axis in I2 chip (the 50% EEAR of PSF is $\sim 14''$ there) and remains unresolved. About 300 counts from it were collected in the observation. No significant variations were detected in its lightcurve. It has a very hard X-ray spectrum that is very flat in the 1 - 10 keV (a power law fit yields a photon index of $0.27^{+0.25}_{-0.23}$). The region around NGC 3861 was detected as a hot spot in the *ASCA* temperature map of A1367 (private communication with E. Churazov). A spectrum with a shape so flat cannot be fitted well with spectra of X-ray binaries (usually ~ 8 keV Bremsstrahlung model). Moreover, the expected 0.3 - 10 keV luminosity of the X-ray binaries in NGC 3861 is 5.2×10^{40} ergs s^{-1}, simply scaled by the X-ray-to-optical luminosity ratio derived for the bulge of M31. This value is only $\sim 10\%$ of the observed luminosity of NGC 3861.

The spectrum of NGC 3861 can be fitted well if we contribute the hard X-ray emission to an absorbed nucleus. We used a power law to fit the hard component and a 8 keV Bremsstrahlung (following S01) to fit the soft component. Besides the Galactic absorption, we set an intrinsic absorption for the hard component. It is found that if the intrinsic absorption is around 6 (4 - 9) $\times10^{22}$ cm^{-2}, the fit is good ($\chi^2 \sim 22/18$) and the photon index is ~ 1.7, which is typical for AGN. The photon index is $1.7^{+0.5}_{-0.6}$ if the absorption is fixed at 6×10^{22} cm^{-2}. The spectrum of NGC 3861 and this best-fit model are shown in Fig. 5. The 2 - 10 keV luminosity of the hard component is $\sim 3\times10^{41}$ ergs s^{-1}. This amount of luminosity and absorption, imply that NGC 3861 is a low luminosity Seyfert II galaxy. The 0.3 - 10 keV luminosity of the soft component is 5.3×10^{40} ergs s^{-1}, consistent with the scaling value from its optical luminosity (5.2×10^{40} ergs s^{-1}). The optical spectrum of the nucleus was obtained with the 60-inch telescope in Mt. Hopkins (private communication with P. Berlind and K. Rines). It shows some activity but not strong, with

moderate [N II] lines but no Hα line.

7) NGC 3861B

In this observation, only $\sim$ 70 counts were collected. We simply used a thermal Bremsstrahlung with a temperature fixed at 8 keV (following S01) to fit the spectrum because of the limited statistics. The fit is acceptable and the derived L_x is $\sim 5\times10^{40}$ ergs s^{-1} (0.3 - 10 keV), which is $\sim$ 4 times the scaled value from its optical luminosity (based on X-ray-to-optical luminosity ratio of the bulge of M31). This might imply that there is another X-ray emission component besides the binary one. Nevertheless, the statistics of the data do not allow us to explore it further. If a power law is used to fit its spectrum, the photon index is $2.6^{+1.6}_{-1.0}$ and the derived L_x is 5×10^{40} ergs s^{-1} (0.3 - 10 keV).

8) NGC 3860

This *Chandra* observation clearly reveals two X-ray components in NGC 3860, a bright central point source and a diffuse extension. The latter has been discussed in paper I. It may be the thermal halo of NGC 3860 with a temperature of $\sim$ 0.7 keV. The position of the bright X-ray point-like source agrees with the optical nucleus of NGC 3860. The upper limit of the size is $\sim 1.0h^{-1}_{0.5}$ kpc. About 350 counts from it were collected. Its spectrum can be fitted well by a power law with $\Gamma=1.44^{+0.19}_{-0.18}$ (χ^2 = 6.2/13). The derived L_x is 1.4×10^{41} ergs s^{-1} in the 0.5 - 10 keV band (1.0×10^{41} ergs s^{-1} in the 2 - 10 keV band). No significant variations in its lightcurve were found. The weak Hα emission observed by Kennicutt, Bothun & Schommer (1984) rules out the possibility of a starburst nucleus. Thus, it is most likely a LLAGN (e.g., Ho 1999). There is a correlation between L_X and L_α for powerful Seyfert 1 nuclei, quasars and some type of LLAGNs (e.g., Ho et. 2001). The nucleus of NGC 3860 also falls on that line (Fig. 2 in Ho et al. 2001), which strengthens our conclusion above.

5. Other point sources

5.1. QSOs

There are three known QSOs (source 11 - 13 in Fig. 2) in the point sources detected. Their properties, including the best fits of their spectra, are listed in Table 4. Their spectra can all be fitted well by a power law modified with the Galactic absorption. Among them, the X-ray emission from the z=2.205 QSO Arp & Gavazzi, 1984) is first reported. The first one (source 11 or EXO 1141.3+2013) is the second brightest X-ray source after 3C 264 in the field. There is an emission line around 4.8 keV in its spectrum (Fig. 6). An inclusion of a gaussian for this line reduces

χ^2 significantly (at a confidence level of $\gtrsim$ 99%; $\Delta\chi^2$ = 9.6 for two additional free parameters). The best-fit of line centroid is $4.87^{+0.07}_{-0.03}$ keV. If the optical redshift 0.335 is adopted, the emitting wavelength in the rest frame would be $6.50^{+0.09}_{-0.05}$ keV, consistent well with iron Kα fluorescence line. The equivalent width of this line is $0.8^{+0.5}_{-0.4}$ keV. We checked the *Chandra* lightcurves of all three QSOs and found no significant variations.

The first two (source 11 and 12) may be radio-quiet QSOs since they have not yet been detected in radio. Moreover, the rather steep X-ray spectra of them ($\Gamma > 2.1$ in 90% confidence levels) are more consistent with the spectra of radio-quiet QSOs (Reeves & Turner 2000). The third one was detected in radio and has a flat radio spectrum (Arp & Gavazzi, 1984). The X-ray spectra of all of them show no intrinsic absorption, which implies that they are not type II QSOs.

5.2. Others

As we mentioned earlier, most of the bright point sources have optical counterparts in DSS II blue image. We also did spectral analysis for the point sources with enough counts ($>$ 50 counts). The spectra of 19 bright sources were fitted and the results are listed in Table 2. Most of them have spectra with photon indices around 1.7 - 2.0. Thus, they may be AGNs. We also checked the variability of bright sources ($>$ 50 counts). A Kolmogorov-Smirnov (K-S) test was used. This test is best for the sources with secular increase or decrease or sudden turn-on or off in the flux, but not good at detecting short-term variations. None of 28 eligible sources ($>$ 30 counts) are found to have significant variations. From Table 2, we can find that at least 8 sources (24, 32, 48-50, 59-61) have intrinsic absorption. The estimated column densities are from 10^{22} to at least 10^{23} cm^{-2}.

6. Log N - Log S relation in the field

Cappi et al. (2001) found source excesses at levels of $\sim 2\,\sigma$ around two z$\sim$0.5 galaxy clusters 3C 295 and RXJ 003033.2+261819. We did a similar analysis for the central field of A1367. We chose the central $8.'3$ square field centered at the aimpoint (a chip size, see Fig. 2), where the sensitivity is the highest, to examine the Log N - Log S relation in the soft band (0.5 - 2 keV) and hard band (2 - 10 keV). The point sources with known origins (associated with member galaxies here) were excluded in computing the Log N - Log S. A power law model (Γ=1.7) with the Galactic absorption is assumed for the sources. The conversion factors are 3.1×10^{-15} ergs cm^{-2} s^{-1} for 1 c/ks in the 0.5 - 2 keV, and 2.4×10^{-14} ergs cm^{-2} s^{-1} for 1 c/ks in the 2 - 10 keV. The results are shown in Fig. 7. The source numbers observed are over 2 times that predicted by the Log N - Log S relations found in the deep fields in both soft and hard bands (Hasinger et al. 1998; Mushotzky

et al. 2000; Giacconi et al. 2001; Tozzi et al. 2001; Brandt et al. 2001). The K-S tests show that the observed Log N - Log S relations and any known ones from deep surveys are quite different ($>$ 0.95). In the soft band, when we move the observed Log N - Log S relations from the deep surveys up to $\sim 2.5\ \sigma$ levels, they begin to be consistent with the observed one. The largest difference is at flux larger than 2×10^{-15} ergs cm^{-2} s^{-1}. We observe 20 sources with fluxes larger than that value, while the Log N - Log S relations from the deep surveys predict 7 - 10 sources. Thus, in the soft band, there is a source excess at a level of $\sim 2.5\ \sigma$. Similarly in the hard band, we detect 16 sources with flux larger than 8×10^{-15} ergs cm^{-2}, while the Log N - Log S relations from the deep surveys predict $\sim$ 6 sources. Thus, in the hard band, there is also a source excess at a level of $\sim$ 2.5 σ.

The source excess observed in A1367 seems similar to what Cappi et al. (2001) found. However, in the case of A1367, since it is much closer than the two z$\sim$0.5 clusters, any galaxies with B less than $\sim 20^{\rm m}$ should be clearly revealed in DSS II blue image. Thus, if the excess sources are related to A1367, then they must be very optically faint (Log($L_B/L_\odot$) $\lesssim$ 8.5). In the sources used to derive the soft band Log N - Log S relation in the central field, the faintest and the brightest sources have X-ray luminosities of 3×10^{39} ergs s^{-1} (0.5 - 2 keV) and 2.5×10^{41} ergs s^{-1} (0.5 - 10 keV) respectively if they are physically located in A1367. For the brightest nine sources in the central field, we have fitted their spectra simply by power law models. The derived photon indices are generally consistent with those of AGN ($\sim$ 1.7; Table 2). Thus, if the excess is due to the sources in A1367, they have to be LLAGNs with low optical luminosities (Log($L_B/L_\odot$) $\lesssim$ 8.5) or even ULXs. Optical identification of all the sources seen in the A1367 field is needed to resolve the difference between the expected excess and that observed.

7. Conclusion

We have reported results from the most complete flux limited sample of X-ray sources in this part of A1367. Ten of twenty-five known member galaxies (Log($L_B/L_\odot$) $\gtrsim$ 9.5) in the *Chandra* field were detected. Thermal halo, X-ray binary and nuclear components are all observed in their spectra. Eight of ten galaxies are point-like sources in this observation and are discussed in the paper.

The radio galaxy 3C 264 (NGC 3862) is found to have a BL Lac-like X-ray spectrum (Γ=2.44$\pm$0.05 in the 0.7 - 9 keV; $\Gamma=2.72^{+0.19}_{-0.18}$ in the 2 - 9 keV). This observation further discovered 2 new AGN/LLAGN (NGC 3861 — absorbed and NGC 3860) and 2 candidates of AGN/LLAGN (CGCG 097-109 and CGCG 097-113), showing that the X-ray observation serves as a powerful way to detect AGN, especially LLAGNs since they usually have weak optical emission lines. It is known that AGNs are rare in the nearby (z $<$ 0.1) cluster of galaxies ($\sim$ 1% by Dressler, Thompson &

Shectman 1985; may be less by Way, Flores & Quintana 1998). There are 25 known member galaxies in the *Chandra* field (from NED). Thus, the observed percentage of AGN/LLAGN in this *Chandra* field ($\gtrsim$ 12%) is much higher than that found by Dressler et al. (1985). However, the limited statistics here make any further discussion impossible at this time.

For early type galaxies, the X-ray luminosities of thermal halos are correlated with the optical luminosities L_B, though dispersion is large (e.g., Canizares, Fabbiano & Trinchieri 1987; Brown & Bregman 1998). Two early type galaxies (NGC 3842 and NGC 3837) were discovered to have soft thermal components, which are explained as thermal halos. They follow the predicted L_X - L_B correlation (e.g., Brown & Bregman 1998). Moreover, we estimated the upper limits of X-ray luminosities of those early type galaxies without detection in the field (Table 1). The derived upper limits are also consistent with the known L_X - L_B correlation. The discovery of the thermal halos in elliptical galaxies NGC 3842 and NGC 3837 (T $\sim$ 0.5 - 0.8 keV), in combination with the discovery of an extended feature associated with NGC 3860 (T $\sim$ 0.5 - 0.9 keV; discussed in paper I), demonstrate that Galactic coronae can survive in the cluster environment (e.g., Vikhlinin et. al 2001). Although we do not know the exact positions of these galaxies along the lines of sight, the fact that NGC 3842 is the cD galaxy of a galaxy concentration suggests that it should be located close to the bottom of the potential well. Using the β-model fit to the NW subcluster by Donnelly et al. (1998), we derive an ICM density of $\sim 5 \times 10^{-4}$ cm $^{-3}$ surrounding NGC 3842. The ICM surrounding NGC 3842 has a temperature of $\sim$ 4.5 keV (see Fig. 6 in paper I). Thus, the evaporation time-scale is $\sim 10^7$ yr (no matter classical or saturated evaporation; Cowie & Mckee 1977). However, the radiative cooling time-scale — $3M_{gas}kT/2\mu m_p L_X$ — is 2.3×10^8 yr for NGC 3842. Thus, heat conduction at the boundary of NGC 3842 must be suppressed to a factor of $\sim$ 20 for the survival of its thermal halo. This provides an additional evidence for the suppression of heat conductivity in the ICM after the *Chandra* discovery of thermal halos in the two dominant galaxies of Coma (Vikhlinin et. al 2001). A tangled magnetic field is one possible reason for such suppression (e.g. Fabian 1994). When we gather more cases of suppressed heat conduction in ICM, the physics behind this phenomenon will be better understood.

The results presented here are made possible by the successful effort of the entire *Chandra* team to build, launch, and operate the observatory. We are very grateful to the referee - Dr. J. Irwin - for his very valuable comments to improve the manuscript. We are also grateful to W. Forman for many important comments to the manuscript. We acknowledge helpful discussions with G. Fabbiano, J. Huchra, M. Markevitch and A. Vikhlinin. This study was supported by NASA contract NAS8-38248.

REFERENCES

Arp, H., Gavazzi, G. 1984, A&A, 139, 240

Bechtold, J. et al. 1983, ApJ, 265, 26 (B83)

Brandt, W. N. et al. 2001, AJ, in press, also astro-ph/0108404

Bridle, A. H., Vallée, J. P. 1981, AJ, 86, 1165

Brown, B. A., Bregman, J. N. 1998, 495, L75

Canizares, C. R., Fabbiano, G., Trinchieri, G. 1987, ApJ, 312, 503

Cappi, M. et al. 2001, ApJ, 548, 624

Ciliegi, P., Bassani, L., Caroli, E. 1995, ApJ, 439, 80

Cowie, L. L., McKee, C. F. 1977, ApJ, 211, 135

Crane, P. et al. 1993, ApJ, 402, L37

Donnelly, R. H., Markevitch, M., Forman, W., Jones, C., David, L. P., Churazov, E., Gilfanov, M. 1998, ApJ, 500, 138

Dow, K. L. & White, S. D. M. 1995, ApJ, 439, 113

Dressler, A., Thompson, I. B., & Shectman, S. A. 1985, ApJ, 288, 481

Elvis, M., Schreier, E. J., Tonry, J., Davis, M., Huchra, J. P. 1981, ApJ, 246, 20

Fabbiano, G., Zezas, A., Murray, S. S. 2001, ApJ, 554, 1035

Fabian, A. C. 1994, ARA&A, 32, 277

Freeman, P. E., Kashyap, V., Rosner, R., Lamb, D. Q. 2002, ApJS, in press, also astro-ph/0108429

Gavazzi, G., Contursi, A. 1994, AJ, 108, 24, (GC94)

Giacconi, R. et al. 2001, ApJ, 551, 624

Grebenev, S. A., Forman, W., Jones, C., Murray, S. S. 1995, ApJ, 445, 607 (G95)

Hasinger, G., Burg, R., Giacconi, R., Schmidt, M., Trümper, J., Zamorani, G. 1998, A&A, 329, 482

Ho, L. C. 1999, ApJ, 516, 672

Ho, L. C. et al. 2001, ApJ, 549, L51

Kennicutt, R. C., Bothun, G. D., Schommer, R. A. 1984, AJ, 89, 1279

Kubo, H. et al. 1998, ApJ, 504, 693

Lazzati, D., Campana, S., Rosati, P., Chincarini, G., Giacconi, R. 1998, A&A, 1998, 331, 41 (L98)

Marshall, F. E., Mushotzky, R. F., Boldt, E. A., Holt, S. S., Rothschild, R. E., Serlemitsos, P. J. 1978, Nature, 275, 624

Mushotzky, R. F., Cowie, L. L., Barger, A. J., Arnaud, K. A. 2000, Nature, 404, 459

Nandra, K., Pounds, K. A. 1994, MNRAS, 268, 405

Reeves, J. N., & Turner, M. J. L. 2000, MNRAS, 316, 234

Sakelliou, I., Merrifield, M. R. 1998, MNRAS, 293, 489

Sambruna, R. M., Eracleous, M., Mushotzky, R. F. 1999, ApJ, 526, 60

Sarazin, C. L., Irwin, J. A., & Bregman, J. N. 2001, ApJ, in press, also astro-ph/0104070, (S01)

Schommer, R. A., Bothun, G. D. 1983, AJ, 88, 577

Sun, M., Murray, S. S. 2002, ApJ, accepted (paper I)

Tozzi, P. et al. 2001, ApJ in press, aslo astro-ph/0103014

Vikhlinin, A., Markevitch, M., Forman, W., & Jones, C. 2001, ApJL, 555, 87

Way, M. J., Flores, R. A., Quintana, H. 1998, ApJ, 502, 134

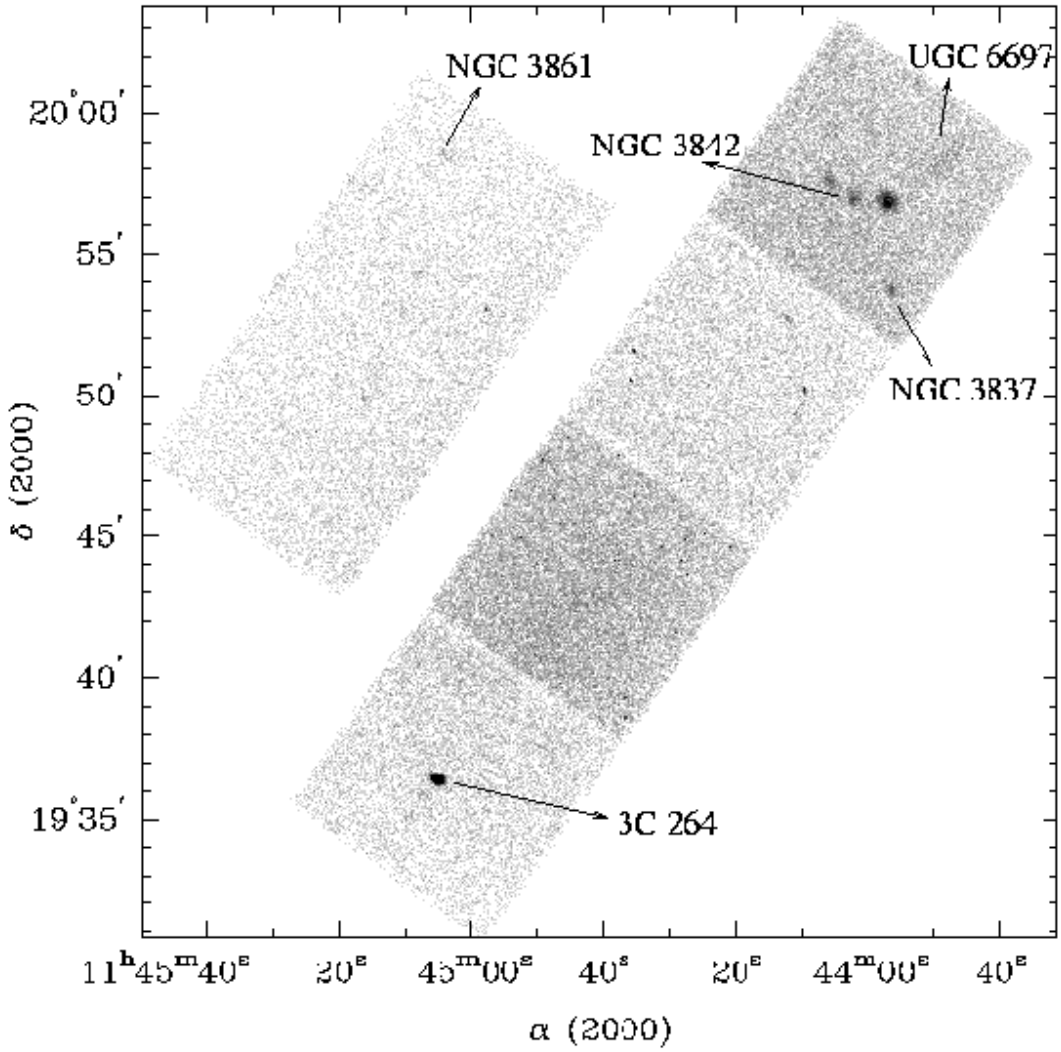

Fig. 1.— The 0.3 - 8 keV photon image, binned to 2″ pixels. The detected sources are shown in Fig. 2.

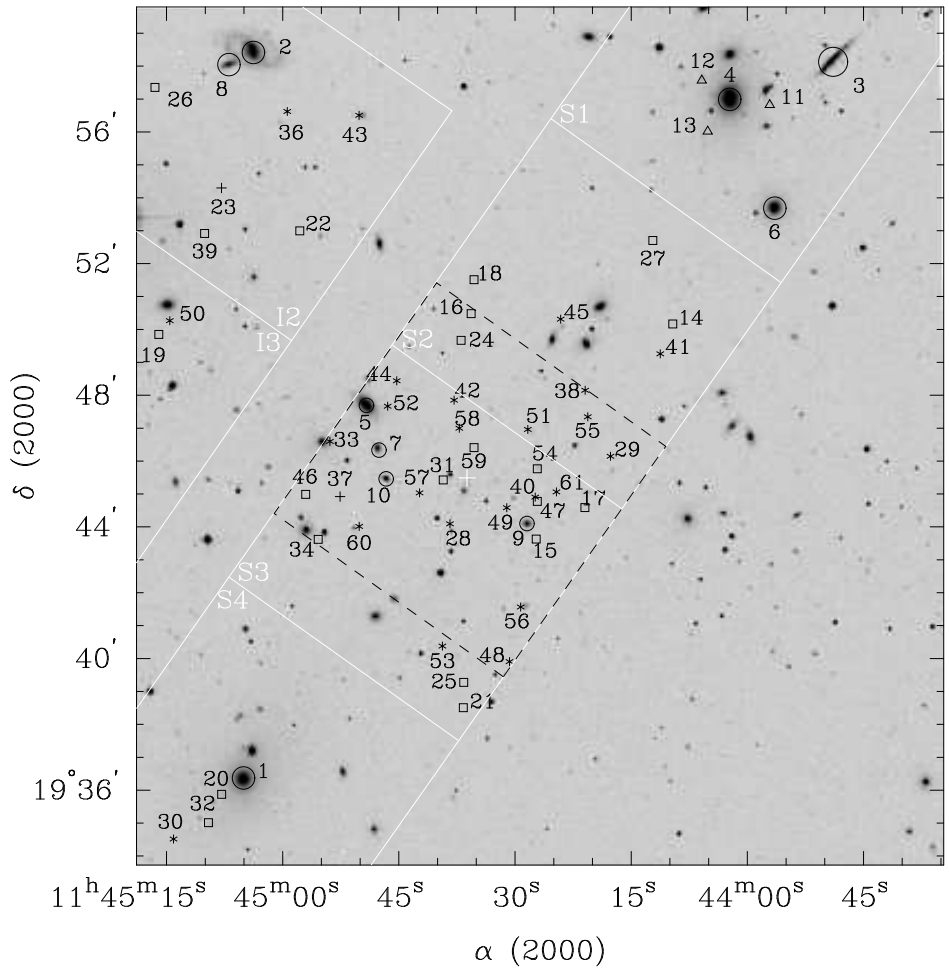

Fig. 2.— The detected point-like sources (59 in total; source 35 is out of the figure and has no counterpart in either DSS II or GC94) overlaid on the DSS II image. To show the crowded sources in the central field clearly, we do not include the whole field. Source 1 - 10 are sources associated with known member galaxies (represented by circles). Source 3 and 7 (UGC 6697 and NGC 3860B) are actually extended sources. Source 5 (NGC 3860) has a point-like and an extended component. We include them to show all 10 member galaxies detected in X-ray. They are numbered according to their X-ray luminosities from high to low. Source 11 - 13 are known QSOs (represented by triangles). They are numbered according to their observed fluxes from high to low. Source 14 - 61 are sources with unknown origins (many of them may be AGNs based on their *Chandra* spectra), including the sources that have DSS II counterparts (represented by small boxes), the sources that have radio counterparts in GC94 (represented by crosses), and the sources without counterparts in both DSS II and GC94 (represented by asterisks). They are also numbered according to the observed fluxes from high to low. The white lines delineate the CCD chips. The white cross represents the aimpoint. The box in dashed-line is the one-chip region around the aimpoint that we chose to measure the Log N - Log S (§6).

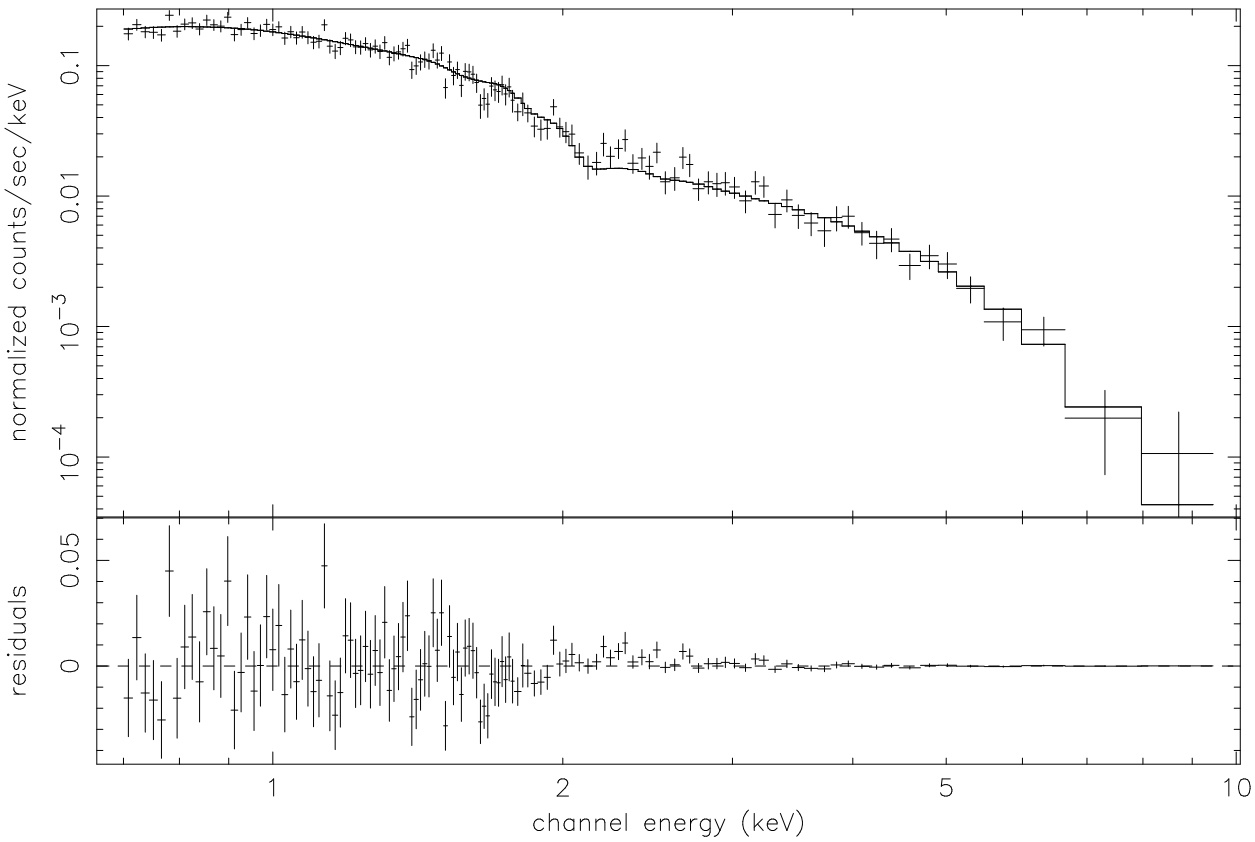

Fig. 3.— The *Chandra* spectrum of NGC 3862 with the best-fit model (a power law with Γ=2.44$\pm$0.05 modified by the Galactic absorption).

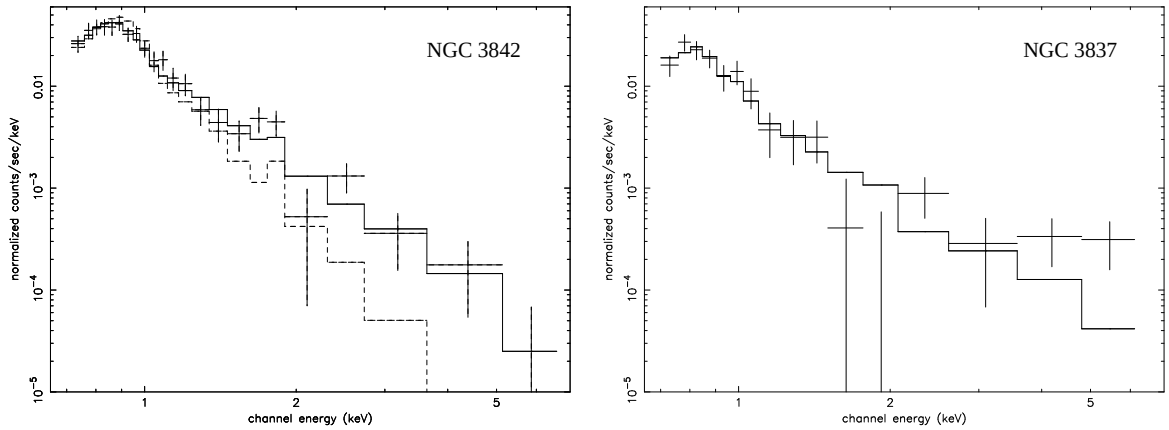

Fig. 4.— **Left**: the *Chandra* spectrum of NGC 3842 with the best-fit model (MEKAL + Bremsstrahlung, see text), while the dashed line demonstrates the single MEKAL fit that fails to describe the hard X-rays; **Right**: the *Chandra* spectrum of NGC 3837 with the best-fit model (MEKAL + Bremsstrahlung, see text). Both spectra clearly show at least two components.

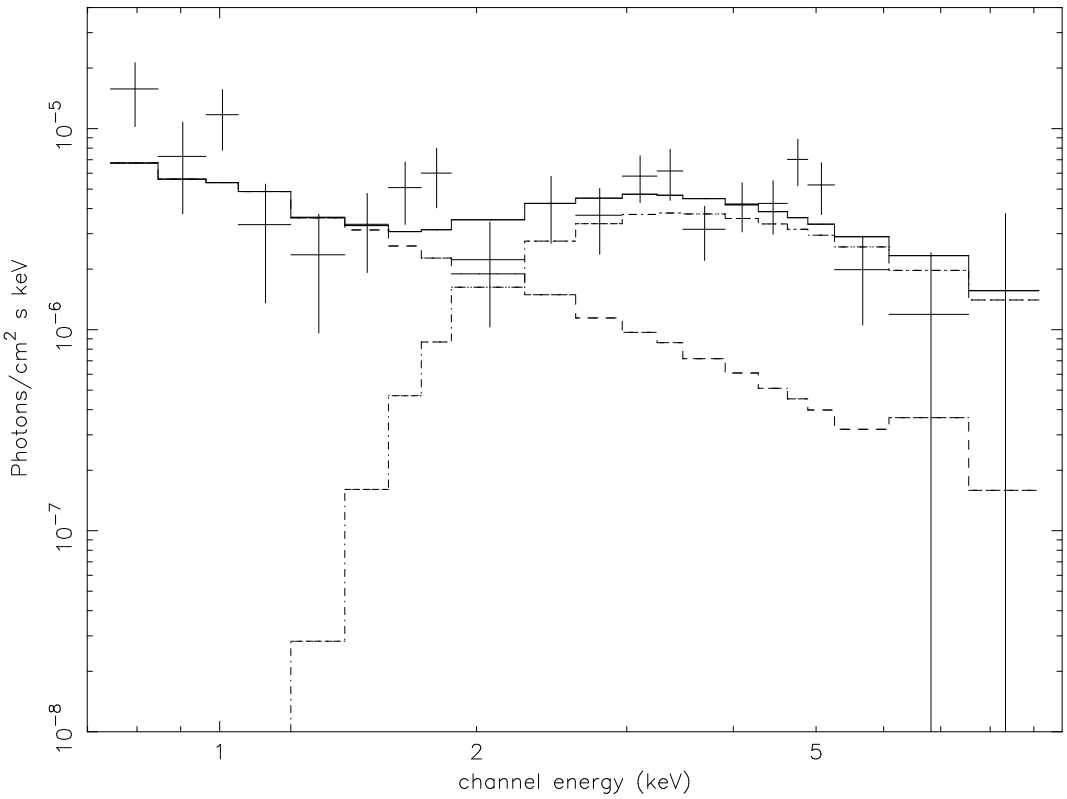

Fig. 5.— The *Chandra* spectrum of NGC 3861 with the best-fit of the intrinsic absorption model. The dashed line represents the Bremsstrahlung for the soft component while the dash-dot line represents the absorbed power law for the hard component. The solid line is their combination.

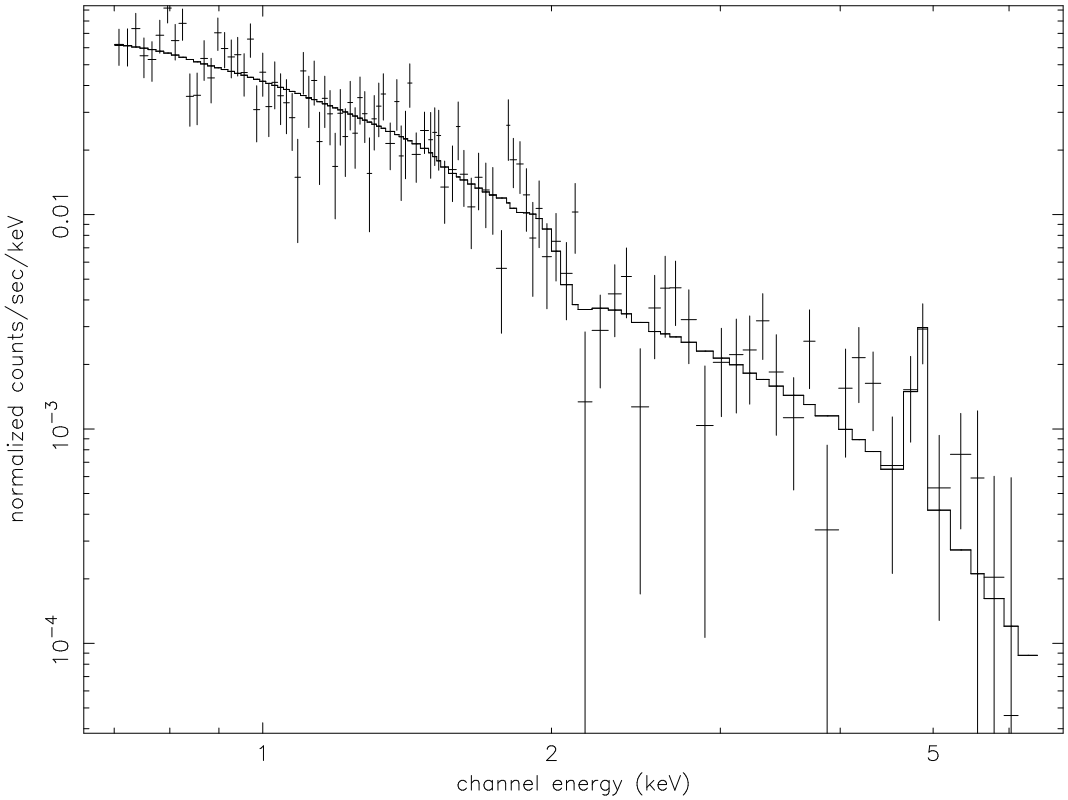

Fig. 6.— The *Chandra* ACIS-S1 spectrum of z=0.335 QSO (EXO 1141.3+2013; source 11 in Fig. 2) with the best fit (see Table 4). The red-shifted iron Kα line is obvious.

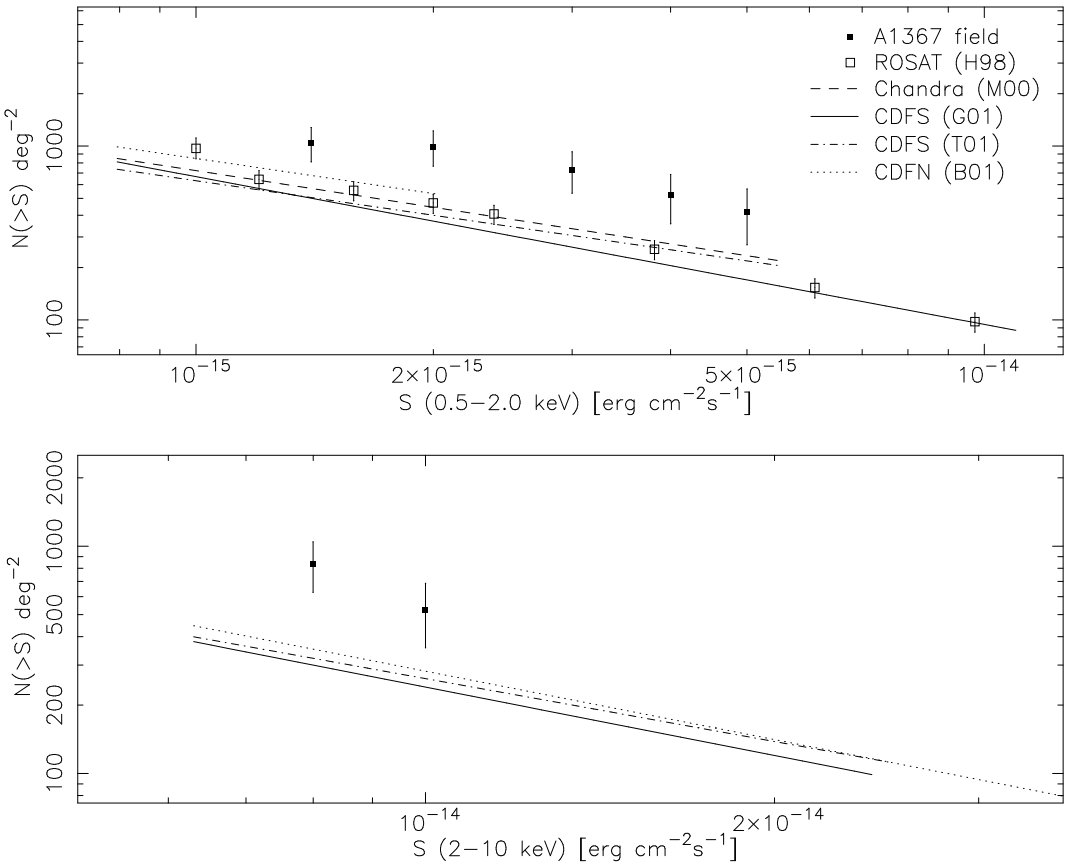

Fig. 7.— The soft band (0.5 - 2 keV) and hard band (2 - 10 keV) Log N - Log S relations observed in the central 8.′3 square region (1 chip size, see Fig. 2) compared to the results from deep surveys: H98 - deep PSPC+HRI observations by Hasinger et al. (1998); M00 - deep *Chandra* observation by Mushotzky et al. (2000); G01 - *Chandra* deep field south (CDFS) 120 ks by Giacconi et al. (2001); T01 - CDFS 300 ks by Tozzi et al. (2001); B01 - *Chandra* deep field north (CDFN) 1 Ms by Brandt et al. (2001). The point sources associated with the member galaxies are excluded in computing the observed Log N - Log S. There are source excesses in the central field both in soft and hard band on levels of $\sim 2.5\ \sigma$.

TABLE 1

MEMBER GALAXIES[a] IN THE ACIS FIELD

Name[b]	R.A.[c] (2000)	DEC.[c] (2000)	Type	Velocity (km/s)	Log ($L_B/L_\odot$)	Radio[d]	Infrared	Previous X-ray[e]	θ^f_{off} (′)	*Chandra* [g]	Count rate (c/ks) (0.5 - 2 keV)[h]	Count rate (c/ks) (2 - 7 keV)[h]
NGC 3842	11:44:02.2	19:56:59	E	6316±9	11.24	65	-	Gp8	13.9	4	27.57	-
UGC 6697*	11:43:49.1	19:58:06	Irr	6725±2	11.00	58	IRAS 11412+2014	Gp4	16.7	3	28.07	-
NGC 3862 (3C 264)	11:45:05.0	19:36:23	E, RG	6511±6	10.99	84	-	Ge28, Gp24	11.4	1	408.26	48.99
NGC 3861	11:45:03.8	19:58:26	Sb	5085±2	10.94	83	IRAS 11424+2015	Gp23	14.1	2	6.04	5.82
NGC 3860*	11:44:49.17	19:47:44.4	Sa	5595±8	10.72	76	IRAS 11422+2003	Ge22, Gp18	3.8	5	11.51	2.35
NGC 3837	11:43:56.3	19:53:42	E	6130±10	10.64	59	-	Ge1, Gp5	12.4	6	11.39	-
ARK 319	11:45:14.9	19:50:44	E	7739±7	10.61	-	-	Gp26	10.5	< 0.8 (2.1)	-	-
NGC 3841	11:44:02.2	19:58:19	E	6356±7	10.54	-	-	-	15.1	< 2.1 (2.8)	-	-
NGC 3860B*	11:44:47.6	19:46:22	Irr	8293±9	10.53	75	-	Gp18*	2.8	7	3.57	-
NGC 3844	11:44:00.8	20:01:46	S0/a	6834±18	10.49	-	-	-	18.2	< 2.3 (2.5)	-	-
CGCG 097-109	11:44:28.38	19:44:08.7	E	6823±19	10.42	-	-	-	2.8	9	1.17	-
IC 2955	11:45:03.9	19:37:14	E	6511±5	10.37	-	-	-	10.6	< 2.1 (2.4)	-	-
CGCG 097-124 NED01	11:44:56.9	19:43:55	S0	7756±28	10.34	-	-	-	5.1	< 0.4 (1.1)	-	-
NGC 3845	11:44:05.5	19:59:46	S0	5692±26	10.27	-	-	-	15.9	< 2.2 (2.6)	-	-
CGCG 097-101	11:44:19.0	19:50:41	S0	6399±23	10.26	-	-	-	6.5	< 0.8 (1.7)	-	-
CGCG 097-090	11:43:57.5	19:57:13	S0	6148±179	10.22	-	-	-	14.8	< 4.7 (5.1) [i]	-	-
CGCG 097-113	11:44:46.6	19:45:30	S0	6419	10.18	-	-	-	2.5	10	0.54	-
NGC 3861B	11:45:06.9	19:57:59	Sc	5970±75	10.18	-	-	-	14.4	8	2.00	-
CGCG 097-118	11:44:52.2	19:36:36	S0	6556	10.12	-	-	-	9.7	< 1.6 (2.1)	-	-
CGCG 097-105	11:44:20.8	19:49:34	S0/a	5522±34	10.09	-	-	-	5.4	< 0.7 (1.7)	-	-
2MASXi J1144481+193451	11:44:48.1	19:34:51		6256±214	9.95	-	-	-	11.1	< 1.7 (2.1)	-	-
2MASXi J1144365+194505	11:44:36.6	19:45:06		8230±51	9.92	-	-	-	0.5	< 0.3 (0.7)	-	-
CGCG 097-110	11:44:25.1	19:49:42	S0	4427±32	9.86	-	-	-	4.9	< 0.6 (1.6)	-	-
CGCG 097-119	11:44:47.9	19:41:19	S0/a	4869±35	9.86	-	-	Ge21, Gp17	5.1	< 0.5 (1.0)	-	-
CGCG 097-124 NED02	11:44:57.6	19:44:18		6031±56	9.77	-	-	-	5.2	< 0.4 (0.6)	-	-

[a] The type, velocity and L_B of galaxies are from NED. "-" in the table means no detection.

[b] The galaxies with asterisk are detected as extended sources and were discussed in paper I. NGC 3860 has both point and extended components.

[c] If the galaxy is detected in this *Chandra* observation, the X-ray position is listed. Otherwise, the optical position from NED is listed.

[d] The source number in GC94

[e] The source number in G95; "Gp" means PSPC sources and "Ge" means EHRI sources.

[f] The off-axis angle of the source.

[g] If the galaxy is detected by *Chandra*, we list the source number in Fig. 2. Otherwise, 3 σ upper limits (0.5 - 2 keV, in 10^{40} ergs s^{-1}) on the point-like emission and extended emission (in bracket) are given. The aperture for the point-like emission is set at 90% EEAR. The aperture for the extended emission is set according to the optical galaxy sizes, from 30″ to 2′.

[h] The exposure maps used are computed relatively to the aimpoint. Thus, the correction on vignetting has been included. For NGC 3860, both point and extended components are included.

[i] This galaxy is close to the bright X-ray source EXO 1141.3-2013 so that the upper limits are relatively large.

TABLE 2

POINT SOURCES WITH UNKNOWN ORIGINS[a]

#[b]	R.A.[c] (2000)	DEC.[c] (2000)	θ_{off}^{d} (′)	Count Rate (c/ks) (0.5 - 2 keV)[e]	Count Rate (c/ks) (2 - 7 keV)[e]	Γ[f]	Comment[g]
14	11:44:09.46	19:50:10.8	7.8	13.71	2.25	$2.03^{+0.22}_{-0.21}$	Gp10, Ge7, Lp26
15	11:44:27.16	19:43:38.6	2.8	11.8	3.07	$1.76^{+0.14}_{-0.13}$	Gp11*, Ge14
16	11:44:35.59	19:50:30.0	5.0	9.50	1.29	$2.15^{+0.26}_{-0.24}$	
17	11:44:20.84	19:44:36.0	3.7	8.37	2.25	$1.68^{+0.15}_{-0.16}$	Gp11
18	11:44:35.22	19:51:31.9	6.0	6.89	1.92	$1.67^{+0.28}_{-0.25}$	Gp12, Ge17, Lp10
19	11:45:16.1	19:49:50	10.3	6.89	1.66	$1.9^{+0.5}_{-0.4}$	
20	11:45:07.5	19:35:51	12.1	4.95	2.38	1.0±0.3	
21	11:44:36.55	19:38:30.9	7.0	5.74	1.43	1.8±0.3	Gp13
22	11:44:57.78	19:53:01.8	9.1	5.35	1.44	$1.8^{+0.6}_{-0.4}$	
23	11:45:07.8	19:54:18	11.5	4.62	1.18	$1.7^{+0.6}_{-0.4}$	Gp26, Lp15
24	11:44:36.91	19:49:41.1	4.2	2.95	2.73	$1.4^{+0.6}_{-0.4}$	NH: $1.0^{+0.8}_{-0.5}\times10^{22}$ cm^{-2}
25	11:44:36.53	19:39:16.9	6.2	3.90	1.74	1.5±0.3	
26	11:45:15.8	19:57:24	15.1	5.62	-	1.9±0.5	Gp25, Lp25
27	11:44:12.02	19:52:42.8	9.2	4.92	-	$1.9^{+0.9}_{-0.6}$	Ge8
28	11:44:38.34	19:44:05.9	1.5	2.26	0.78	$1.7^{+0.4}_{-0.3}$	
29	11:44:17.57	19:46:09.3	4.4	1.95	0.76	$1.4^{+0.9}_{-0.7}$	
30	11:45:13.4	19:34:34	14.2	-	-	-	2.39 c/ks
31	11:44:39.19	19:45:26.4	0.7	1.56	0.59	1.4±0.4	
32	11:45:09.5	19:35:01	13.1	-	2.11	-	
33	11:44:53.83	19:46:36.7	4.3	1.48	0.39	-	
34	11:44:55.33	19:43:37.7	4.9	1.83	-	$2.2^{+1.8}_{-0.9}$	
35	11:45:29.3	19:53:59	15.1	1.83	-	-	
36	11:44:59.4	19:56:39	12.3	-	-	-	1.79 c/ks
37	11:44:52.58	19:44:55.5	3.9	1.64	-	$2.2^{+0.8}_{-0.6}$	
38	11:44:20.82	19:48:10.1	4.5	1.05	0.45	-	
39	11:45:10.1	19:52:56	11.0	-	-	-	1.50 c/ks
40	11:44:27.36	19:44:54.0	2.1	1.01	0.37	-	
41	11:44:11.07	19:49:17.0	7.0	1.29	-	-	
42	11:44:37.81	19:47:51.3	2.4	0.87	0.40	-	
43	11:44:50.1	19:56:32	11.4	-	-	-	1.10 c/ks
44	11:44:45.20	19:48:28.2	3.7	1.08	-	-	
45	11:44:23.93	19:50:21.6	5.6	1.02	-	-	
46	11:44:56.91	19:44:59.5	4.9	0.97	-	-	
47	11:44:27.00	19:44:48.0	2.3	0.96	-	-	
48	11:44:30.67	19:39:54.2	5.8	-	0.86	-	
49	11:44:31.06	19:44:35.5	1.5	-	0.86	-	
50	11:45:14.6	19:50:17	10.2	-	0.79	-	
51	11:44:28.24	19:46:59.0	2.3	0.73	-	-	
52	11:44:46.40	19:47:40.7	3.3	0.72	-	-	
53	11:44:39.38	19:40:23.1	5.2	-	-	-	0.72 c/ks
54	11:44:27.00	19:45:48.8	2.2	0.66	-	-	
55	11:44:20.49	19:47:21.3	4.1	-	-	-	0.49 c/ks
56	11:44:29.12	19:41:34.7	4.3	-	-	-	0.48 c/ks
57	11:44:42.24	19:45:03.0	1.5	0.45	-	-	
58	11:44:37.09	19:46:58.9	1.5	-	-	-	0.39 c/ks
59	11:44:35.14	19:46:25.5	0.9	-	0.37	-	
60	11:44:50.05	19:44:01.6	3.6	-	0.35	-	
61	11:44:24.53	19:45:04.7	2.8	-	0.35	-	

[a] The point sources associated with known member galaxies and QSOs (source 1 - 10 and 11 - 13) are not included in this table. They are

discussed in §4 and §5.1 respectively. The detection threshold is 3 σ in the 0.5 - 7 keV energy band. None of the sources show significant X-ray variation.

[b] The source number in Fig. 2.

[c] The uncertainties of the positions are $\sim 0.5''$ near the aimpoint, up to $4''$ in the farthest positions to the aimpoint.

[d] The off-axis angle of the source.

[e] The exposure maps used are computed relatively to the aimpoint. Thus, the correction on vignetting has been included.

[f] The results of the power law fits. Only sources with more than 50 counts were analyzed. The absorption is fixed at the Galactic value unless the spectrum strongly suggests intrinsic absorption, e.g., source 24.

[g] "Gp" means *ROSAT* PSPC sources detected by G95; "Ge" means EHRI sources detected by G95; "Lp" means *ROSAT* PSPC sources detected by L98.

Note: For the point sources only seen in the broad band image, only the count rates in the 0.5 - 7 keV band are given.

TABLE 3

POINT SOURCES DETECTED BY PREVIOUS MISSIONS[a]

B83 #[b]	G95 #[c]	L98 #[d]	*Chandra* result[e]
Bp1	Ge2, Gp6	Lp28	11
Bp2	Ge5, Gp9	-	12
Bp3	-	-	-
Bp5	-	-	-
Bp8	Ge28, Gp24	Lp1	1
-	Ge1, Gp5	Lp21	6
-	Ge3	-	-
-	Ge6	-	-
-	Ge8	-	27
-	Ge10	-	-
-	Ge11	-	-
-	Ge13	-	-
-	Ge15	-	-
-	Ge18	-	-
-	Ge20	-	-
-	Ge24	-	-
-	Ge25, Gp23	Lp9	2 & 8
Be14 (ex)	Ge26	-	-
-	Gp20	-	22
	Gp4	Lp7 (ex)	3 (ex)
-	Gp8	Lp28	4
-	Gp11	-	17
-	Gp13	-	21
	Gp25	Lp25	26
	Gp26	Lp15	19
Be2 (ex)	Ge7, Gp10	Lp26	14
Be8 (ex)	Ge22 (ex), Gp18	Lp16 (ex)	5

[a] Only the "point sources" claimed previously in the field are included (27 of 47) and unless pointed out, all the sources are point-like. "(ex)" means extended. "-" means no detection, while blank means not in the field.

[b] Source number in B83; the first letter of the source ID indicates the author. 'p' means point-like and 'e' means extended.

[c] Source number in G95; 'p' means PSPC source and 'e' means EHRI source.

[d] Source number in L98; 'p' means PSPC source.

[e] The source number in Fig. 2

TABLE 4

THE KNOWN QSOS DETECTED BY *Chandra* [a]

#[b]	R.A. (J2000)	DEC. (J2000)	z	Radio[c]	V (mag)	Counts	Γ[d]	L_X^e ergs s^{-1}	Comment[f]
11	11:43:56.90	19:56:49.7	0.335	-	18.5	3280	$2.29^{+0.14}_{-0.13}$	1.1×10^{44}	Ge2, Gp6, EXO 1141.3+2013
12	11:44:05.69	19:57:35.8	0.946	-	18.5	690	$2.6^{+0.5}_{-0.4}$	1.6×10^{44}	Ge5, Gp9
13	11:44:05.30[g]	19:56:03.0[g]	2.205	67	21	200	$2.0^{+1.0}_{-0.6}$	5.6×10^{44}	First detected

[a] The coordinates, redshift and V magnitude of QSOs are from NED and Arp & Gavazzi (1984).
[b] The source number in Fig. 2
[c] The source number in Table 2 of GC94
[d] The best-fit photon index of a power law modified by the Galactic absorption. We fitted the 0.75 - 9 keV spectra. If only 2 - 9 keV spectra are fitted, the results are quite similar to ones shown here.
[e] In the 2 - 10 keV band
[f] Previous detections if have
[g] This coordinate is obtained from Arp & Gavazzi (1984). The coordinate from *Chandra* is within $1.5''$ of this position.